Determination of electron density and temperature in a capacitively coupled RF discharge in neon by OES complemented with a CR model

2010 J. Phys. D: Appl. Phys. 43 505203

(http://iopscience.iop.org/0022-3727/43/50/505203)

IOP PUBLISHING JOURNAL OF PHYSICS D: APPLIED PHYSICS

J. Phys. D: Appl. Phys. **43** (2010) 505203 (11pp) doi:10.1088/0022-3727/43/50/505203

Determination of electron density and temperature in a capacitively coupled RF discharge in neon by OES complemented with a CR model

Z Navrátil[1], P Dvořák[1], O Brzobohatý[2] and D Trunec[1]

[1] Department of Physical Electronics, Faculty of Science, Masaryk University, Kotlářská 2, 611 37 Brno, Czech Republic

[2] Institute of Scientific Instruments of the ASCR, v.v.i., Academy of Sciences of the Czech Republic, Královopolská 147, 612 64 Brno, Czech Republic

E-mail: zdenek@physics.muni.cz

Received 21 July 2010, in final form 19 October 2010
Published 2 December 2010
Online at stacks.iop.org/JPhysD/43/505203

Abstract

A method of determination of electron temperature and electron density in plasmas based on optical emission spectroscopy complemented with collisional–radiative modelling (OES/CRM) was studied in this work. A radiofrequency (13.56 MHz) capacitively coupled discharge in neon at 10 Pa was investigated by intensity calibrated optical emission spectroscopy. The absolute intensities of neon transitions between 3p and 3s states were fitted with a collisional–radiative (CR) model in order to determine the electron temperature and electron density. Measuring techniques such as imaging with an ICCD camera were adopted for supplementary diagnostics. The obtained results were compared with the results of compensated Langmuir probe measurement and one-dimensional particle-in-cell/Monte Carlo (PIC/MC) simulation.

The results of OES/CRM and PIC/MC method were in close agreement in the case of electron temperature in the vicinity of a driven electrode. The determined value of electron temperature was about 8 eV. In bulk plasma, the measured spectra were not satisfactorily fitted. In the case of electron density only relative agreement was obtained between OES/CRM and Langmuir probe measurement; the absolute values differed by a factor of 5. The axial dependence of electron density calculated by PIC/MC was distinct from them, reaching the maximum values between the results of the other two methods. The investigation of power dependence of plasma parameters close to the driven electrode showed a decrease in electron temperature and an increase in electron density together with increasing incoming RF power. The calculated spectra fitted very well the measured spectra in this discharge region.

(Some figures in this article are in colour only in the electronic version)

1. Introduction

Radiofrequency (RF) capacitively coupled discharges are widely used in industrial applications for thin film deposition, etching, cleaning, surface modification, in high power lasers, as analytical sources, light sources, etc [1]. However, precise measurement of the basic plasma parameters such as electron density and electron temperature or electron distribution function is still demanded. Although the use of Langmuir probe in RF discharges is well established, it is still limited to low-pressure plasmas, risking the plasma disturbance and suffering with low signal-to-noise ratio for highly energetic electrons, which have a low concentration but high impact on plasma processes. On the other hand, optical emission spectroscopy (OES) seems to overcome all these drawbacks. However, in order to derive the plasma parameters

from the measured optical emission spectra, a relatively complicated collisional–radiative (CR) modelling is generally needed.

In the case of rare gases, the capacitively coupled RF discharge has been extensively studied in helium and argon, but less often in neon. Electron distribution function (EDF) has previously been measured with a Langmuir probe in argon and helium [2]. Anisotropy of electron energy distribution function was measured by an electrostatic energy analyser in asymmetric helium RF discharges [3]. Thomson light scattering was adopted for low electron temperature and density measurement in helium RF discharges [4]. Transition between α and γ mode of RF discharges in argon was investigated in [5]. Time-averaged axial potential profile was measured with the electrostatic probe in symmetric RF discharge in neon [6]. Paper [7] compared EDFs measured in a discharge centre at different pressures (0.1–0.8 Torr) in neon, argon and xenon. EDF in capacitive RF discharges in molecular gases was also investigated (see e.g. [8, 9] for nitrogen).

The cited papers show the necessity of knowledge of EDF for understanding capacitive discharges, including understanding of heating mechanisms and prediction of reactions induced by electron collisions. Further important information concerning the physics of capacitively coupled discharges can be obtained by methods that enable measurements with a high temporal resolution. Uncompensated electric probes enable measurement of plasma potential changes occurring during one RF period [10, 11]. OES with a high temporal resolution brings an illustrative look into the processes occurring in each RF period, including discharge heating in α and γ modes [12], generation of electron beams by sheath expansion [13] and field reversal during sheath collapse [14]. Despite the fact that these measurements brought numerous facts on the time development of capacitive discharges, they did not provide information concerning EDFs, electron concentration or temperature. Therefore, measurement of EDFs based on OES, which is noninvasive and potentially enables a high temporal resolution, is still desired.

Computer simulation, especially CR modelling, has become widely used for diagnostics of various types of discharges [15–17]. The method of electron temperature measurement based on a CR model for argon was reported, e.g., in [18]. Trace rare gases optical emission spectroscopy (TRG-OES), based on the addition of a small admixture of rare gas into the studied plasma and evaluation of plasma parameters from the best fit between the measured and CR model calculated relative emission intensities, was reviewed in [19]. Comparative diagnostics of helium and argon microwave plasmas at a pressure of 1–5 Torr utilizing CR model, OES and probe measurement was published in [20]. Statistical analysis of reconstruction of EDF in the positive column of neon dc discharge from the emission spectra was presented in [21]. Application of particle-in-cell/Monte Carlo method (PIC/MC) for investigation of plasma was published in [22–24].

In this work a method of the determination of electron temperature and density from temporally averaged optical emission spectra is developed for neon plasma and compared with the results from Langmuir probe measurement and PIC/MC simulation. The paper is organized as follows: details of experimental apparatus, OES and Langmuir probe diagnostics are given in section 2. CR model and PIC/MC approach are described in sections 3 and 4, respectively. The results obtained with the above mentioned methods are presented, compared and discussed in section 5. Conclusions are given in section 6.

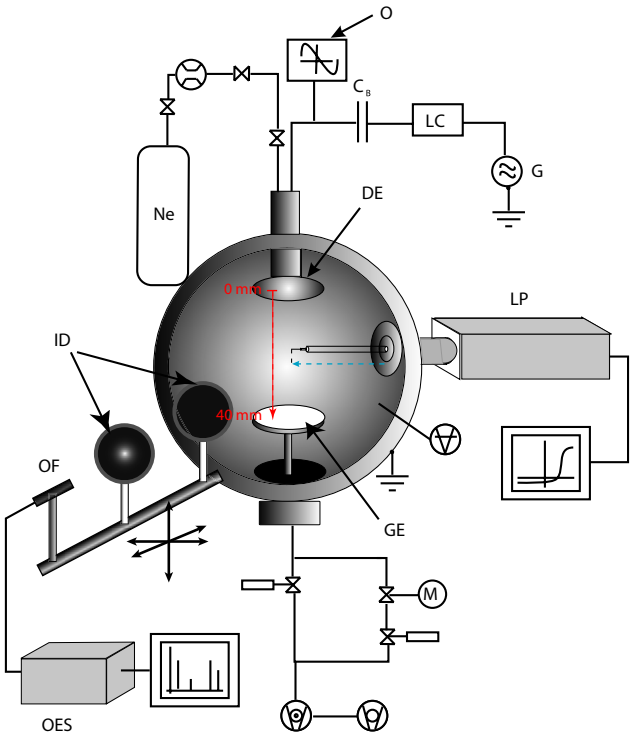

Figure 1. The scheme of experimental set-up: DE and GE—driven and grounded movable electrode, G—13.56 MHz generator, O—oscilloscope, OF—optical fibre, ID—iris diaphragms, OES—Jobin Yvon FHR 1000 spectrometer, LP—Langmuir probe.

2. Experimental set-up

The schematic of the experimental set-up is displayed in figure 1. The RF discharge was generated in a grounded stainless-steel vacuum chamber with an inner diameter of 33 cm. Two parallel plate circular electrodes with a diameter of 80 mm were placed 40 mm apart. The upper electrode (located at position 0 mm), embedded in a grounded ring, was capacitively coupled to a RF sinusoidal voltage generator (13.56 MHz, maximum power 50 W, maximum applied voltage 470 V_{pp}). The lower electrode (located at position 40 mm) was grounded. The dc self-bias on the powered electrode varied within −130 to −300 V showing an asymmetry of the discharge.

The vacuum chamber was pumped down using a turbomolecular pump to an ultimate pressure of 5×10^{-5} Pa and then filled with neon gas of research purity 5.0 up to pressures of 5–15 Pa. The discharge was sustained in flowing regime with gas flow rate approximately 5 sccm. The butterfly valve

between the chamber and the pump controlled the pumping speed, allowing the pressure to be set independently of the flow rate. The pressure in the chamber was measured by a MKS Baratron. A large window, with diameter 7 cm, enabled the observation of the discharge.

2.1. Langmuir probe measurement

Electron energy distribution function, electron concentration, mean electron energy and mean (dc) plasma potential were measured using a compensated Langmuir probe (ESPion, Hiden Analytical). The probe consisted of a 1 cm long platinum wire, radius 190 μm, connected to a control unit and computer. RF voltage including higher harmonic frequencies was passively compensated [25]. Eventual disturbance of plasma potential due to high sheath resistivity was compensated by means of a reference probe [26]. Electron energy distribution functions were calculated from a second derivative of the probe characteristics by the well-known Druywestein formula. If EDFs had Maxwellian shape, the electron concentration and mean energy were calculated from a linear fit to a logarithm of measured probe characteristics in order to exclude the impact of noise produced by numerical calculation of the second derivative. Analogically, when it was possible to describe EDF by so-called general distribution, an appropriate function was fitted to the logarithm of the measured data. The general distribution f_g is described by the relation

$$f_g(E) = C_g\, n_e\, E^{1/2} \exp\left\{-\frac{E^\kappa}{2\kappa\, E_p^\kappa}\right\}$$

where n_e, E and E_p are the electron concentration, energy and the most probable energy, respectively. C_g is a constant depending only on E_p and κ. κ describes the shape of the EDF. For $\kappa = 1$ or $\kappa = 2$ the general distribution is identical to Maxwellian or Druywestein distribution, respectively. When EDFs had another shape, electron concentration and mean energy were calculated by integration of EDFs obtained by the Druywestein formula. At the pressure 10 Pa the measured EDFs were similar to Maxwellian EDF. The statistical error of electron temperature and density determined from repeated probe measurement was below 5% and 4%, respectively.

2.2. Optical emission spectroscopy

The emission of radiation from the discharge was studied by optical spectroscopy in the UV/VIS spectral range (300–750 nm). The spatial resolution of the measurement was achieved by two iris diaphragms, mounted with optical fibre on a movable table in front of the chamber window. The light coming from a narrow cone going through the whole discharge diameter, but with a distinct axial position between the electrodes, was taken out with the diaphragms and optical fibre and analysed with a Jobin Yvon FHR 1000 spectrometer with a CCD detector (focal length 1 m, grating 2400 gr mm^{-1}). The spectra were integrated over many periods of RF signal. An Oriel tungsten halogen lamp was used to calibrate the fibre irradiance. Original uncertainty of the lamp intensity was 2%. A new recalibration with 5% uncertainty revealed as much as 10% difference in the calibrations.

The emission coefficient ϵ_{ij} of specific transition $i \to j$, integrated over the lineshape, was derived from the fibre irradiance. If the cylindrical symmetry of plasma with uniform radial profile for region between the electrodes can be assumed

$$\epsilon_{ij}(r) = \begin{cases} \epsilon_{ij}, & r \leqslant R, \\ 0, & r > R, \end{cases}$$

where ϵ_{ij} is the emission coefficient of unit discharge volume defined as

$$\epsilon_{ij} = \frac{1}{4\pi} n_i A_{ij} \Lambda_{ij} \hbar\omega_{ij},$$

where n_i is the population of excited state i, A_{ij} and Λ_{ij} Einstein coefficient and so-called escape factor of spontaneous emission, respectively, and $\hbar\omega_{ij}$ is the corresponding photon energy, then the irradiance of the optical fibre ('detector') is

$$I_{ij} = \frac{1}{S_{det}} \int_{V_{pl}} \int_{S_{det}} \frac{\epsilon_{ij}(r)}{\rho^2} \mathrm{Acc}(\theta)\, \mathrm{d}V_{pl}\, \mathrm{d}S_{det},$$

where ρ is the distance of the plasma element $\mathrm{d}V_{pl}$ from the detector part $\mathrm{d}S_{det}$, θ is the angle of incidence and $\mathrm{Acc}(\theta)$ represents the fibre acceptance function, determined experimentally. The escape factor Λ_{ij} approximates the reduction of emitted photons due to reabsorption [27, 28]. Under the above-mentioned considerations the emission coefficient can be taken out from the integral. In our case, the plasma region contributing through the iris diaphragms to the irradiation of fibre aperture was assumed to have a cylindrical shape with length $2R = 110$ mm and diameter 5 mm. Constant value of emission coefficient along this length and diameter was assumed and taken into calculations.

Supplementary temporally and spatially resolved, but spectrally unresolved, measurement of discharge emission of radiation was carried out with an intensified CCD camera PI-MAX 1024RB-25-FG-43, controlled by a ST-133 controller and working in image mode. The temporal resolution was 5 ns and the spatial resolution 0.3 mm.

3. Collisional–radiative model

The CR model used in this work was described in detail in [29], where a method of determination of reduced electric field strength in the positive column of neon dc glow discharge was developed. Basically, comparing the measured spectra of the discharge with the spectra calculated with the CR model by the least-squares method, the plasma parameters as reduced electric field strength, electron temperature or electron density may be determined from the best fit.

In this work, Maxwellian electron distribution function (Maxwellian EDF) was assumed for calculation of rates of collisional processes. Other distribution functions, such as, so-called, bi-Maxwellian EDF, general EDF f_g, or product of PIC/MC simulation could be included in the calculations. The comparison between the measured and calculated spectra was performed on the basis of $1/I$-weighted sum of squares, where I stands for intensity. Since the measured spectra

were determined in absolute values of emission coefficient (in $\mathrm{W\,m^{-3}\,sr^{-1}}$), no scaling factor between the measured and calculated intensities was needed. In contrast, a strong dependence of absolute intensity on the electron density increased the sensitivity of the fit to the electron density. Twenty-six transitions of neon were taken for fitting.

In the CR model 30 excited states of neon, arising from $2p^5 3s$, $2p^5 3p$, $2p^5 4s$ and $2p^5 3d$ configurations, were considered. Various collisional, radiative and also diffusion processes were taken into account: electron impact excitation out of the ground state and 3s states and de-excitation to these states, electron impact excitation transfer between 3s levels, spontaneous emission of radiation, radiation trapping, electron impact ionization of the ground-state and metastable atoms, chemoionization, associative ionization, two-body and three-body collisions with ground-state neon atoms or diffusion of metastable-state atoms to the wall. The radiation trapping was incorporated by means of so-called trapping factors (or escape factors, respectively). In their calculations, Voigt profile with Doppler, Stark, natural and resonance broadening components was assumed for lineshapes.

The Einstein coefficients, cross-sections, rate coefficients and other data were taken primarily from [29]. The rate constants for electron impact-induced excitation transfer between 3s states were adopted from [30]. The original sources of Einstein coefficients and oscillator strengths were [31] and [32], respectively. For 3s–3p transitions, the accuracy of Einstein coefficients was below 10% (class B), the calculated oscillator strengths differed from experimental data no more than 10%, mostly they were 3% higher [32]. This is in agreement with our comparison of both data sources. However, for 3p–3d transitions, with only indirect influence on fitted 3s–3p lines, the differences between the data sources reach 30–40%. Accuracy up to 50% (class D) is reported in [31].

4. Particle-in-Cell/Monte Carlo model

One-dimensional (1D) electrostatic PDP1 code [33, 34] was modified and employed for the study of various plasma parameters of the RF discharge in neon, e.g. of spatial distribution of plasma density and EDF. The PDP1 code applied the approach of PIC/MC methods. Motion of the charged particles in the electric field was solved using the PIC method [22, 23] incorporating a self-consistent solution of the Newton motion equations

$$m_i \boldsymbol{a}_i = q_i \boldsymbol{E}, \qquad i = 1, \ldots, N,$$

where m_i, $\boldsymbol{a}_i$, q_i, $\boldsymbol{E}$ and N denote the particle mass, acceleration, charge, electric field strength and the number of charged particles in the system, respectively, together with the Poisson equation

$$\nabla^2 \varphi = -\rho/\varepsilon_0,$$

in which φ and ρ stand for the electric field potential and the charge density, respectively. The equations of motion were solved numerically employing the well-known leap-frog (explicit) method. To reduce a huge number of charged particles in the studied plasma the so-called computer particles were brought into play [22]. The number of such computer super-particles was then $\approx 10^4$.

Collisions of charged particles with the neutral atoms were considered in our model using a MC method [24, 33]. Free flight time of charged particles was calculated using the null-collision method. The initial velocities of particles, e.g. after ionization collisions, were also generated using the MC method. Elastic, excitation and ionization collisions were considered for the electrons and the elastic and charge transfer collisions for the ions. The methods briefly described above are nowadays well utilized in computer simulations of plasma [35–37].

The model system was set in accordance with the experimental set-up. It consisted of two parallel electrodes having the same diameter of 8 cm. The distance between the electrodes was set at 40 mm. One electrode was powered by RF voltage, the second electrode was grounded. The frequency f of the power source was 13.56 MHz, the voltage amplitude V_0 was 300 V. The pressure p of the neutral gas was 10 Pa or 15 Pa, respectively. Since with the 1D model a negative self-bias could not be modelled, it was introduced into the model as a boundary condition [38].

The boundaries of our computer model were given with the electrodes, where secondary electron emission and recombination occurred. Generally, secondary electron yields for incident electrons and ions, γ_e and γ_+, respectively, differ. A secondary electron yield γ_e depends on electron energy and incident angle. On the other hand a secondary electron yield γ_+ for low energetic ions, i.e. in the case of Auger emission, is dependent only on the type of ion [39, 40]. Assuming constant values γ for ions and electrons (independent of projectile energy and incident angle) the problem was simplified in our model. The distribution of initial velocities of the secondary electrons was chosen arbitrarily as half-Maxwellian with the temperature $kT = 1$ eV. The performed tests proved that this choice of initial secondary electron temperature ($kT \in 0.5$–3 eV) did not influence the results significantly (not presented in this paper).

5. Results and discussion

5.1. Axial dependence

The axial electron temperature dependences determined in the discharge at pressure 10 Pa and RF power 50 W from OES/CRM method, Langmuir probe measurement and PIC/MC simulation are shown in figure 2. In the case of OES/CRM method, two dependences are shown: with metastable densities determined from the CR model and with densities set to fixed values $1.4 \times 10^{15}\,\mathrm{m^{-3}}$ and $7.0 \times 10^{15}\,\mathrm{m^{-3}}$ for $1s_3$ and $1s_5$ states, respectively, according to absorption measurement of $1s_5$ population (not presented in this paper). The Maxwellian distribution function was assumed in these calculations. Since PIC/MC simulation generally predicted non-Maxwellian EDF, both effective temperature T_{eff} calculated as two-thirds of the mean electron kinetic energy, and T_{high} from a slope of EDF at electron

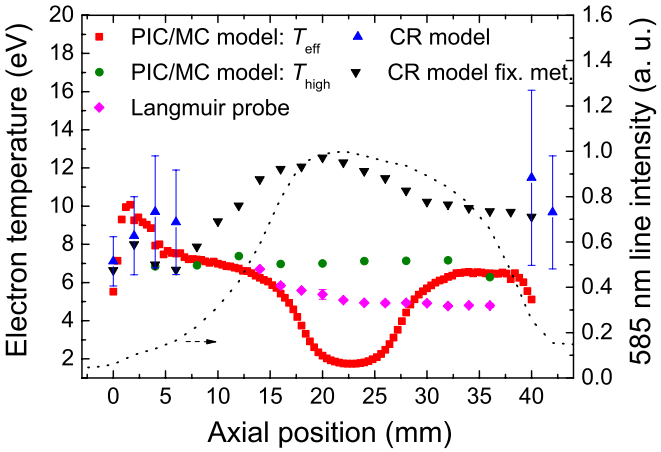

Figure 2. The electron temperature versus axial position for pressure 10 Pa as determined by various methods: PIC/MC T_{eff}, T_{high}—effective temperature determined from mean electron kinetic energy and slope of EDF at electron energies above 16 eV, respectively, Langmuir probe measurement, CR model with metastable density determined from the model, CR model with metastable density set according to absorption measurement. Axial profile of intensity of the 585 nm line (dotted line) is shown to clarify the axial position: 0 mm—driven electrode, 40 mm—grounded electrode.

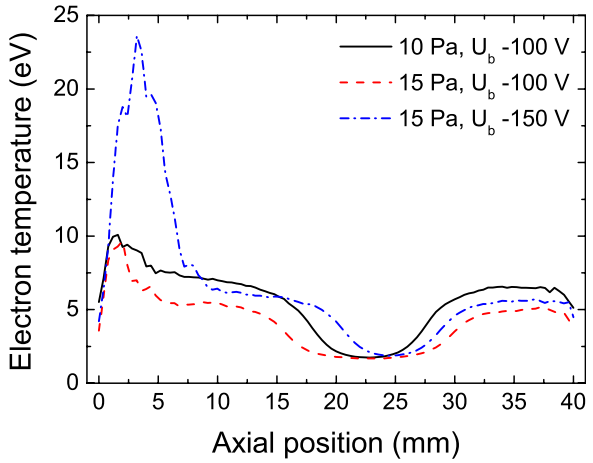

Figure 3. The electron temperature determined from PIC/MC model for pressures 10 Pa and 15 Pa and bias −100 V and −150 V, respectively. The temperature is only effective and it is calculated from the mean electron kinetic energy.

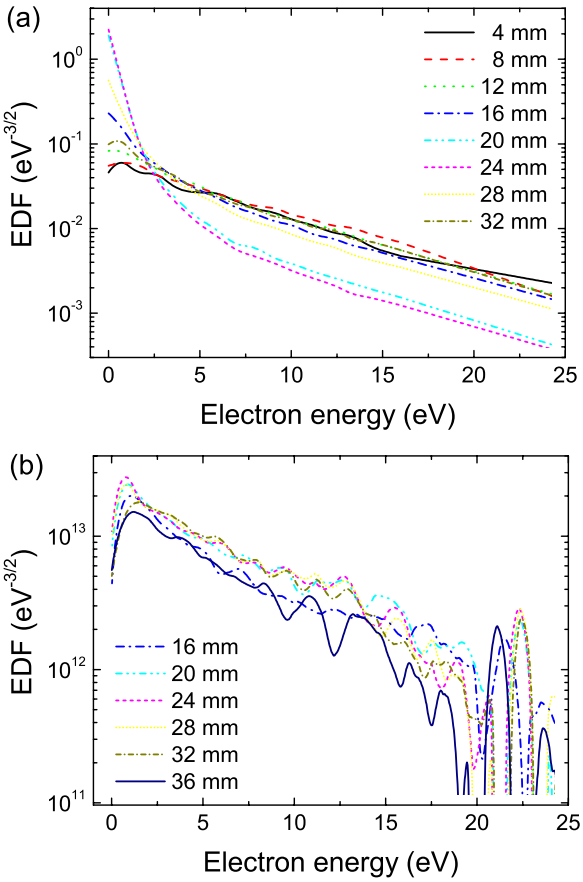

Figure 4. EDF at different axial positions, as determined from (*a*) 1D PIC/MC simulation for pressure 10 Pa and bias −100 V and (*b*) Langmuir probe measurement. The EDF determined in PIC/MC simulation was Maxwellian at the electrodes and deviated from this distribution going into the bulk plasma. The measured EDF was Maxwellian at all measured positions.

energies above 16 eV are displayed. There is obviously good agreement between OES/CRM method and PIC/MC simulation close to the driven electrode (axial position 0–7 mm in the plots). Both dependences of the OES/CRM method gave similar values of electron temperature within the error, since calculated and fixed metastable densities were of the same order. There was also a perfect agreement between the spectra measured with OES and the spectra calculated with the CR model (see section 5.2 for more information). The Langmuir probe could not be used in the RF sheath. However, going into the bulk plasma, considerable discrepancy between the measurement and simulations was observed. According to PIC/MC simulations, T_{eff} decreases to about 2 eV at positions 20–25 mm, while T_{high} stays constant at approximately 7 eV. Neither the result of OES/CRM nor of the Langmuir probe were in agreement with this prediction. Although the Langmuir probe registers particularly the development of T_{eff}, the temperature determined from the probe changes only slowly around 5 eV. The optical spectra depend mostly on T_{high}, but the electron temperature values determined from the OES/CRM method were considerably higher. Also the calculated spectra did not satisfactorily fit the measured spectra in the bulk plasma. Although PIC/MC simulation predicts electrons with a temperature about 10–20 eV under similar discharge conditions due to stochastic heating (see figure 3 and also next), they are expected just conversely close to the driven electrode.

The differences between Langmuir probe measurement and the PIC/MC model can be understood by directly comparing the EDFs (see figure 4). The PIC/MC simulation generally predicts bi-Maxwellian, or a more complicated EDF. Close to the electrode, PIC/MC expects only electrons with higher temperature, $T_{high} \approx 7$ eV, and the EDF is Maxwellian. Going into the bulk plasma a group of low energetic electrons with temperature ≈0.7 eV appears, but T_{high} remains the same, though the density of electrons with this temperature decreases. This behaviour of EDF is responsible for the development of T_{eff} observed in figure 2: T_{eff} approaches T_{high} at the

electrodes, but decreases in the middle. The EDF measured by the Langmuir probe was almost Maxwellian at all measured positions (see figure 4(*b*)). An only weakly steeper low-energy part of EDF was observed at the discharge centre (positions 20–28 mm). Consequently, the probe measurements did not confirm the bi-Maxwellian character of the EDF. However, the determination of the low-energy part of EDF by a Langmuir probe is known to suffer from several problems [2]. A large number of low-energy electrons, present in the bulk plasma, may be unregistered by the probe. For these reasons, the temperature determined from the probe measurement (see figure 2) does not follow the axial dependence of T_{eff} from PIC/MC simulation with pronounced temperature minimum in the bulk plasma.

The bi-Maxwellian EDF was first observed by Godyak *et al* [41] in argon, employing the Langmuir probe. The origin of bi-Maxwellian EDF is relatively simple. The high-temperature group of electrons gain their energy in the so-called stochastic heating process, in which interactions of electrons with the oscillating plasma sheaths are crucial. This group of electrons has enough energy to enter into inelastic collisions with neutral atoms; furthermore, these electrons can easily overcome the ambipolar potential barrier interacting, therefore, more frequently with the oscillating sheath edges [41].

On the other hand, electrons created in the ionization collisions inside the bulk of the plasma belong to the group of low-temperature electrons. These electrons oscillate in a very weak electric field presented in the bulk of the plasma and hence cannot gain energy to overcome the ambipolar potential barrier on the boundary of plasma sheath and plasma bulk, where there exists a maximal electric field and where stochastic heating takes place [39, 41–43]. Thermalization of these electrons occurs only due to the elastic collisions with neutral atoms, which become important at higher pressures.

5.1.1. Influence of EDF type. It is interesting that OES/CRM and PIC/MC methods gave similar temperature values only in the electrode region, where EDF was Maxwellian according to PIC/MC simulations. Considerable attention was therefore paid to describe the electrons of the bulk plasma in the CR model by more sophisticated EDFs. Bi-Maxwellian, general distribution function and also directly the EDF produced by PIC/MC were tested in the CR model to explain the discrepancy between the measured optical spectra and the spectra calculated for temperature expected by other methods. However, no substantial improvement was obtained. Bi-Maxwellian EDF gave a similar value of electron temperature in the high-energy region to Maxwellian EDF. Moreover, it was not possible to let the fitting algorithm change low energy temperature independently, since optical spectra are less sensitive to this parameter through stepwise excitation and de-excitation processes. General distribution function was found to describe the electrons better (evaluated by sum of squared differences in measured and fitted spectra), but only in electrode vicinity, where the deviation from Maxwellian distribution was small. As expected, the use of EDF from PIC/MC simulation did not produce optical spectra similar to the spectra observed by OES.

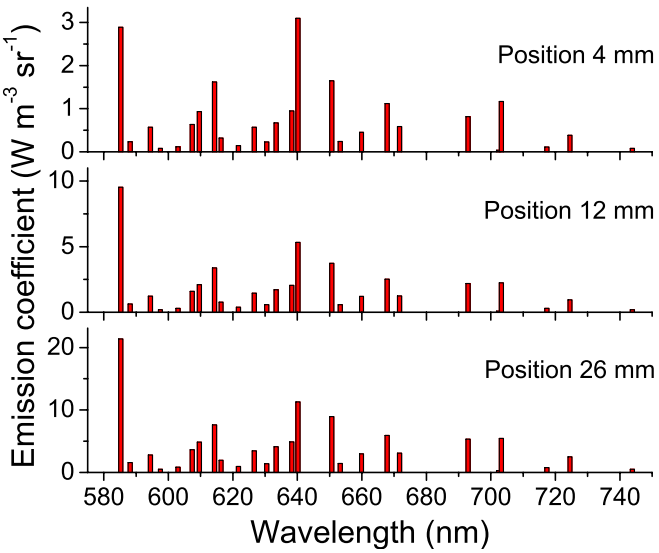

Figure 5. The dependence of measured optical spectra of neon RF discharge at pressure 10 Pa and incoming power 50 W on axial position. The line intensities were integrated over their lineshapes. Note the different scales of vertical axes.

5.1.2. Influence of metastables. In agreement with our previous work [29], the calculated intensities of 3p–3s transitions depended considerably on the populations of metastables. The influence of metastables (and of all states of 3s configuration) on the populations of 3p states is through a stepwise electron impact excitation and it is crucial at low electron energies. At higher electron energies the direct excitation from the ground state becomes the most important. This provides a sensitivity of the spectra to the electron temperature, although excitation energies of 3p states differ by 0.6 eV at most. On the other hand, this requires a reliable cross-sectional data for electron impact excitation out of the ground state to 3s states and out of 3s states. In this work a cross-section for $1s_5$–$2p_9$ transition from [44] was scaled with oscillator strength to obtain a consistent cross-section set for all optically allowed excitations out of 3s states [29]. The uncertainty of the collision cross-sections is about ±30% as determined in [44], but the results of various authors differ by as much as a factor of 3 (compare [44–46]). Moreover, reliable calculation of self-absorption of resonant lines and also of lines originating from transitions between 3p and 3s states is needed.

The dependence of the optical spectra on the axial position is shown in figure 5. Going into the bulk plasma the intensities of individual lines increase at different growth rates. Whilst at axial position 4 mm the line at 640 nm is the most intensive, the line at 585 nm dominates in the spectrum at larger axial distances. Since the upper state of the line at 585 nm ($2p_1$ in Paschen notation) is populated mainly by direct electron impact excitation from the ground state and the upper state of the line at 640 mm ($2p_9$) is populated substantially also by stepwise excitation, the increase in intensity ratio 585 nm/640 nm is interpreted by the CR model as enhancement of electron energies in the discharge middle. However, this is in strong contrast with the decrease in electron temperature predicted by the PIC/MC simulation.

The high values of electron temperature determined by the OES/CRM method in the discharge middle suggest that the relative intensities in the spectra are influenced by other processes. For example, the spectra may be influenced by the absorption of light in the outer regions of the discharge and in the vacuum chamber. Metastable atoms diffuse to the chamber wall and can selectively absorb intensities of transitions ending in metastable states. Since these transitions in the opposite direction are also stimulated by electron impact, their absorption may be misinterpreted as enhancement of direct excitation against the stepwise excitation. A simulation of spatial distribution of metastables in the discharge chamber is needed to analyse the effect of absorption. However, this distribution cannot be determined using the local CR model. For measured metastable densities the escape factor of line 640 nm is ≈0.7. The local CR model predicts even higher metastable densities and the escape factor can reach values ≈0.1. Such small values of escape factors show a large influence of the metastables on the line intensities.

5.1.3. Limitations of PIC/MC code. The 1D PIC/MC model is generally valid in cases where the separation between the electrodes is much smaller than the electrode diameters. In our case the separation was 40 mm and the diameters of the electrodes were only 80 mm. Furthermore, the 1D model is symmetric (both electrodes have the same area) and therefore no self-bias can be observed. This drawback of our PIC/MC simulation code was overcome by introducing the bias voltage artificially. The value of the bias was set to −100 V for pressure 10 Pa in simulations, which was below the experimental value. At −220 V the simulation was unstable. However, as can be seen from figure 3, the bias mostly affects the maximal electron temperature[3] of the beam electrons, but the temperature in the bulk remains approximately the same, and the minimum only shifts in the axial direction.

The discrepancy between measured and simulated EDFs in bulk plasma (the measured EDF was Maxwellian, but the simulated EDF was bi-Maxwellian) may be due to simple incorporation of inelastic collisions. Only total-excitation into 3s state was considered in the model from excitations. For example, superelastic collisions can reasonably modify the shape of EDF. However, the influence of higher excited states on EDF is usually negligible. For better agreement with the experimental data a more complex 2D or 3D model should be employed.

The comparison of determined electron density in the discharge at pressure 10 Pa is shown as a function of axial position in figure 6. The density dependence is different from the intensity development due to spatially varying electron temperature. The relative axial dependences of electron density determined by OES/CRM and the Langmuir probe are rather similar. However, they differ approximately 5× in their absolute values. This can be due to complicated estimation of spatial dependence of emission coefficient. According to optical and probe measurements of radial dependences of involved parameters (electron temperature and density,

[3] We keep using effective temperature ($k_bT = 2/3E_{mean}$), although E_{mean} would be more appropriate in this discussion.

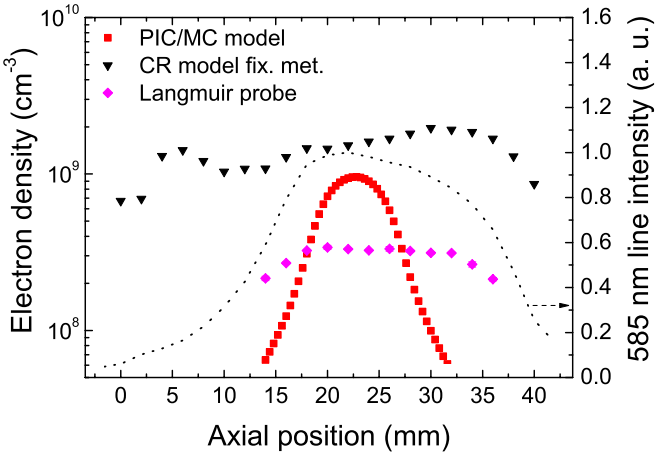

Figure 6. The electron density versus axial position as determined by various methods: PIC/MC simulation, OES/CRM method with metastable density set according to the absorption measurement and Langmuir probe measurement. Axial profile of intensity of the 585 nm line (dotted line) is shown to clarify the axial position: 0 mm—driven electrode, 40 mm—grounded electrode.

discharge intensity) a constant radial profile was assumed for the emission coefficient of plasma region of diameter 110 mm (electrode diameter was 80 mm). However, this assumption is only approximate and at 10 Pa there is still some radiation produced outside this region, which increases the measured intensity and thus also the calculated electron density. The slow decrease in electron density in the sheath observed by the OES/CRM method may also be influenced by this, as well as by reflection of light in the vacuum chamber. Another source of error in the electron concentration determination can be the overestimated absorption of radiation by overestimated concentration of 3s states (see the discussion in section 5.1.2).

The electron density simulated by the PIC/MC method reaches values between the OES/CRM and Langmuir probe results in the bulk plasma. The spatial profile of electron density simulated by the PIC/MC method is sensitive to the self-bias, which is given due to the asymmetry of the electrodes. Better agreement would be achieved by employing a more complex 2D code.

5.1.4. Influence of temporal development. The axially and temporally resolved, but spectrally unresolved, light emission of the discharge measured with the ICCD camera is displayed in figure 7. The light emission is axially and temporally inhomogeneous, although the variation of light intensity through the period is substantially smaller in neon at 10 Pa than at lower pressures [13, 14] or in other gases [14]. In our case the light emission lasted nearly the whole period. Since the light emitted from the discharge was accumulated on the CCD detector over many periods of the RF signal, the obtained results of OES/CRM were averaged over the whole period. For example, the values of electron temperature and density measured at positions close to the electrode do not reflect the conditions in the sheath only, but rather the plasma flooding the region when the sheath collapses. However, the electron temperature and density calculated from temporally integrated

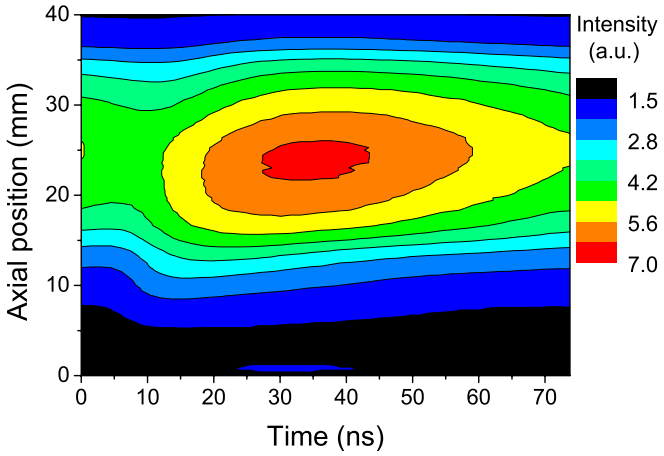

Figure 7. The axially and temporally resolved light emission of RF discharge in neon at 10 Pa, measured with ICCD camera during RF voltage period. The intensity was measured at the discharge centre. The driven electrode is at position 0 mm, grounded electrode at position 40 mm.

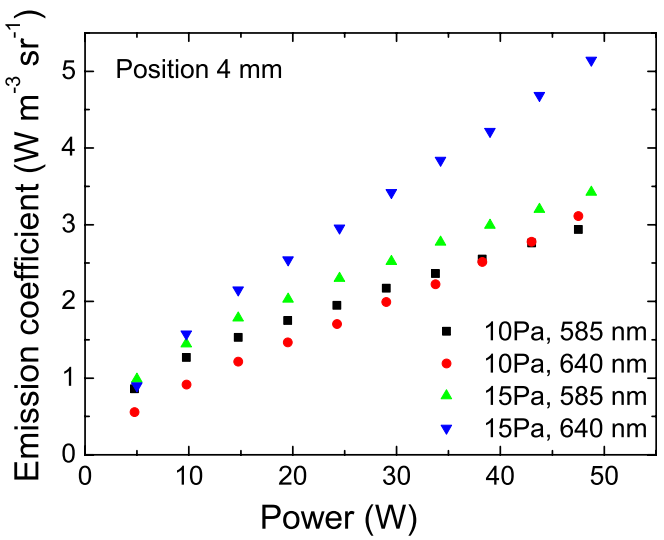

Figure 8. The intensity dependences of two lines at 585 and 640 nm on RF power at position 4 mm from the driven electrode.

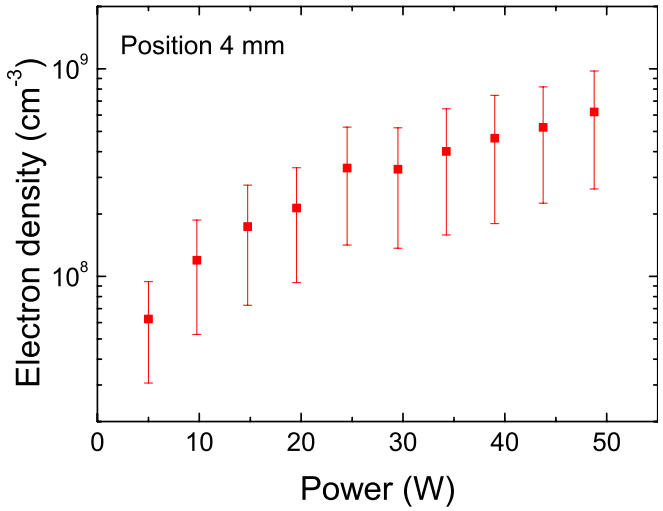

Figure 9. The electron density determined from the spectra taken at position 4 mm from the driven electrode as a function of RF power.

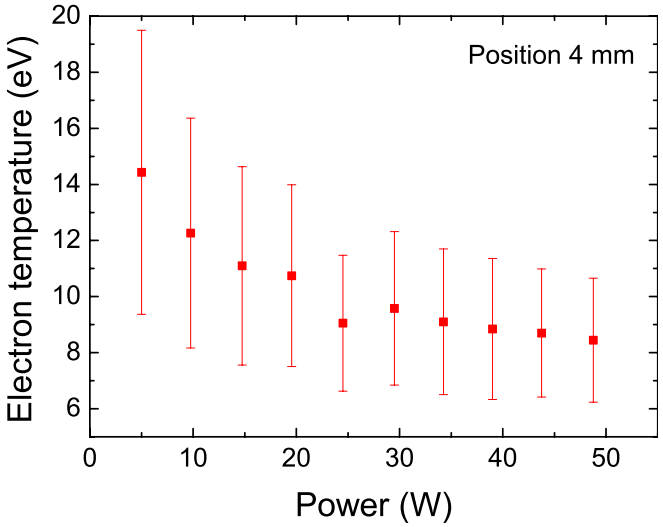

Figure 10. The electron temperature determined from the spectra taken at position 4 mm from the driven electrode as a function of RF power.

intensities need not be simply equal to their temporal mean values, determined, e.g., in PIC/MC simulations.

5.2. *Power dependence*

The agreement of measured and calculated spectra and OES/CRM and the PIC/MC method at positions close to the driven electrode was further analysed by decreasing the incoming RF power. The optical emission spectra were measured at position 4 mm from the driven electrode, the RF power was changed in the range 5–50 W. The metastable density was calculated from the CR model.

The intensities of spectral lines increased monotonically with increasing power. However, they increased in a different way. The dependences of two lines at 585 and 640 nm on RF power are displayed for pressures 10 and 15 Pa in figure 8. It can be seen that whilst the 640 nm line increases nearly linearly with power, the increase in 585 nm line slightly decelerates. This behaviour can be understood considering figures 9 and 10, in which dependences of electron density and electron temperature determined from the spectra are shown (taken at the same axial position 4 mm). It can be seen that with increasing power the electron density increases. This is why intensities of the spectral lines increase. Due to the increasing conductivity of the plasma, electrons gain less energy, which probably causes the decrease in electron temperature. Then, a further decrease in electron temperature affects the excitation of those higher excited states, which are not populated by stepwise excitation through the metastable levels but mostly by direct excitation. This is the case of, e.g., $2p_1$ state, from which the 585 nm line originates.

The examples of fitted spectra for pressure 10 Pa and input RF power 10 W and 50 W, are shown in figures 11 and 12, respectively. Obviously, the agreement between the calculated and measured spectra is appreciably good. This is evidence of

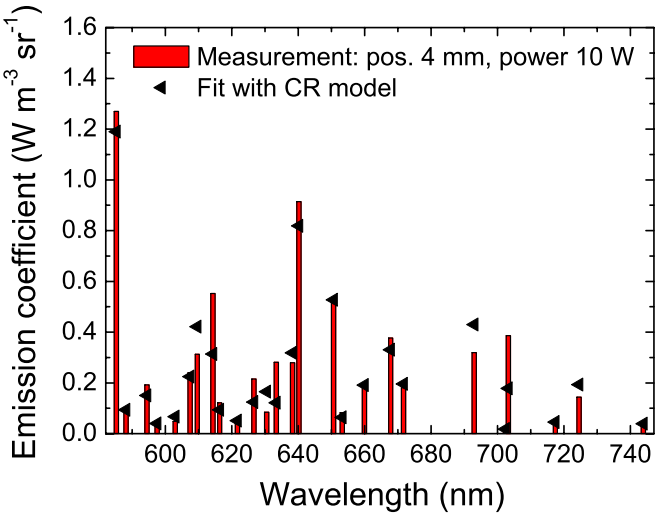

Figure 11. The example of spectra fit at position 4 mm and input RF power 10 W. The electron temperature and density determined from the fit were 12.2 eV and 1.2×10^8 cm^{-3}, respectively.

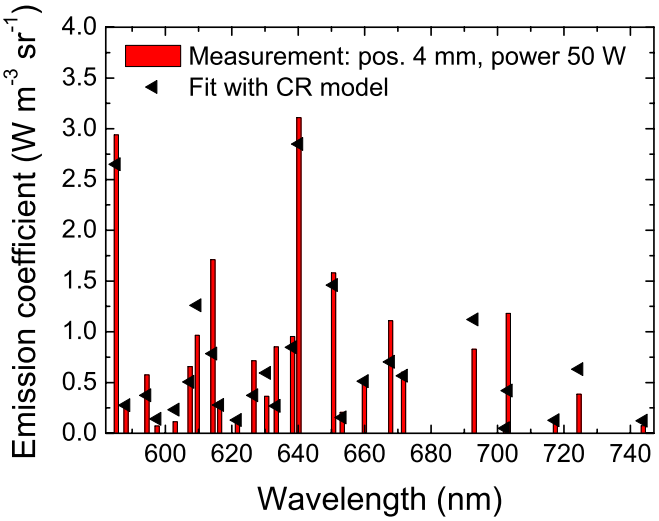

Figure 12. The example of spectra fit at position 4 mm and input RF power 50 W. The electron temperature and density determined from the fit were 8.4 eV and 6.2×10^8 cm^{-3}, respectively.

a valid assumption of Maxwellian EDF and correct description of kinetics in this region.

6. Conclusion

In this work several methods, optical emission spectroscopy with collisional–radiative modelling, Langmuir probe and particle-in-cell/Monte Carlo simulation were applied to the study of a capacitively coupled RF discharge in neon at 10 Pa. The electron density and electron temperature were determined independently by these methods as functions of axial position.

The results of the OES/CRM and the PIC/MC method were in close agreement in the case of electron temperature in the vicinity of the driven electrode. The determined value of electron temperature was about 8 eV. In the bulk plasma, the measured spectra were not satisfactorily fitted. In the case of electron density only relative agreement was obtained between OES/CRM and Langmuir probe measurements; the absolute values differed by a factor of 5. The axial dependence of electron density calculated by PIC/MC was distinct from them, reaching the maximum values between the results of the other two methods. The investigation of power dependence of plasma parameters close to the driven electrode showed a decrease in electron temperature and an increase in electron density with increasing incoming RF power. The measured and calculated spectra agreed very well in this region.

The obtained results suggest that the determination of electron density based on OES with absolute intensity measurement and CR modelling suffers from serious problems. Complicated geometry, unknown radial intensity profile, reflection of light in the chamber, etc—all these attributes make the estimation of absolute emission coefficient and thus also of electron density difficult. On the other hand, the electron temperature is determined mainly from the relative shape of the optical spectra, which is sensitive mostly to the high energetic region of the EDF. Although this sensitivity in the low energetic region of the EDF is increased by the stepwise excitation, fitting problems appear when more free parameters are used to describe the shape of the EDF.

A very important topic is the correct determination of absolute value and spatial profile of neon metastables (or all 3s states). They are not only the initial states, out of which the low energetic electrons populate the studied 3p levels, but they can also alter the spectrum measured by the spectrometer due to radiation trapping. This is in contrast, e.g., with the TRG-OES method, in which the studied emissions may be assumed to be under optically thin conditions [19].

Acknowledgments

The work was supported by the research project MSM 0021622411 of the Ministry of Education of the Czech Republic, grants No 202/09/0800 and No 202/07/1669 of the Czech Science Foundation and by project No KAN 101630651 of the Academy of Sciences of the Czech Republic.

References

[1] Raizer Y P, Shneider M N and Yatsenko M A 1995 *Radio-Frequency Capacitive Discharges* (Boca Raton, FL: CRC Press)

[2] Godyak V A, Piejak R B and Alexandrovich B M 1992 Measurement of electron energy distribution in low-pressure RF discharges *Plasma Sources Sci. Technol.* **1** 36

[3] Okuno Y, Ohtsu Y, Komatsu C and Fujita H 1993 Measurements of electron energy distribution function in an asymmetric radio-frequency discharge plasma *J. Appl. Phys.* **73** 1612

[4] Wesseling H J and Kronast B 1996 Thomson light scattering measurements of electron temperature and density in the α–γ transition of a capacitive rf discharge in helium *J. Phys. D: Appl. Phys.* **29** 1035

[5] Deegan C, Goss J, Vender D and Hopkins M 1999 Measurement of the electron energy distribution function in an argon radio-frequency discharge in the gamma mode *Appl. Phys. Lett.* **74** 1969–71
[6] Kaneda T, Kubota T, Ohuchi M and Chang J S 1990 Time-averaged electric potential profiles in a capacitive-coupling parallel-plate electrode neon gas RF discharge plasma *J. Phys. D: Appl. Phys.* **23** 1642
[7] Kimura T and Ohe K 1997 Pressure dependences of electron energy distribution and power dissipation in symmetrical RF discharges of inert gases *Japan. J. Appl. Phys.* **36** 1274–81
[8] Turner M and Hopkins M 1992 Anomalous sheath heating in a low-pressure RF discharge in nitrogen *Phys. Rev. Lett.* **69** 3511–4
[9] Tatarova E, Stoykova E, Bachev K and Zhelyazkov I 1998 Effects of nonlocal electron kinetics and transition from alpha to gamma regime in an RF capacitive discharge in nitrogen *IEEE Trans. Plasma Sci.* **26** 167–74
[10] Sobolewski M 1995 Electrical characteristics of argon radio frequency glow discharges in an asymmetric cell *IEEE Trans. Plasma Sci.* **23** 1006–22
[11] Dvořák P 2010 Measurement of plasma potential waveforms by an uncompensated probe *Plasma Sources Sci. Technol.* **19** 025014
[12] Schulze J, Donkó Z, Luggenhöelscher D and Czarnetzki U 2009 Different modes of electron heating in dual-frequency capacitively coupled radio frequency discharges *Plasma Sources Sci. Technol.* **18** 034011
[13] Schulze J, Heil B G, Luggenhölscher D, Mussenbrock T, Brinkmann R P and Czarnetzki U 2008 Electron beams in asymmetric capacitively coupled radio frequency discharges at low pressures *J. Phys. D: Appl. Phys.* **41** 042003
[14] Schulze J, Donkó Z, Heil B G, Luggenhölscher D, Mussenbrock T, Brinkmann R P and Czarnetzki U 2008 Electric field reversals in the sheath region of capacitively coupled radio frequency discharges at different pressures *J. Phys. D: Appl. Phys.* **41** 105214
[15] Vlček J 1989 A collisional–radiative model applicable to argon discharges over a wide range of conditions: I. Formulation and basic data *J. Phys. D: Appl. Phys.* **22** 623–31
[16] Golubovskii Y B, Kozakov R V, Nekuchaev V O and Skoblo A Y 2008 Nonlocal electron kinetics and radiation of a stratified positive column of discharge in neon *J. Phys. D: Appl. Phys.* **41** 105205
[17] Zhu X M, Pu Y K, Balcon N and Boswell R 2009 Measurement of the electron density in atmospheric-pressure low-temperature argon discharges by line-ratio method of optical emission spectroscopy *J. Phys. D: Appl. Phys.* **42** 142003
[18] Kano K, Suzuki M and Akatsuka H 2000 Spectroscopic measurements of electron temperature and density in argon plasmas based on collisional–radiative model *Plasma Sources Sci. Technol.* **9** 314–22
[19] Donnelly V M 2004 Plasma electron temperatures and electron energy distributions measured by trace rare gases optical emission spectroscopy *J. Phys. D: Appl. Phys.* **37** R217
[20] Mizuochi J, Sakamoto T, Matsuura H and Akatsuka H 2010 Evaluation of electron energy distribution function in microwave discharge plasmas by spectroscopic diagnostics with collisional–radiative model *Japan. J. Appl. Phys.* **49** 036001
[21] Dodt D, Dinklage A, Fischer R, Bartschat K, Zatsarinny O and Loffhagen D 2008 Reconstruction of an electron energy distribution function using integrated data analysis *J. Phys. D: Appl. Phys.* **41** 205207
[22] Birdsall C K and Langdon A B 1991 *Plasma Physics via Computer Simulation* (Bristol: Adam Hilger)
[23] Hockney R W and Eastwood J W 1988 *Computer Simulation using Particles* (Bristol: Adam Hilger)
[24] Nanbu K 2000 Probability theory of electron–molecule, ion–molecule, molecule–molecule, and Coulomb collisions for particle modeling of materials processing plasmas and gases *IEEE Trans. Plasma Sci.* **28** 971–90
[25] Hopkins M 1995 Langmuir probe measurements in the Gaseous Electronic Conference RF reference cell *J. Res. Natl Inst. Stand. Technol.* **100** 415–25
[26] Kleber J and Overzet L 1999 Sheath resistance measurements in the GEC reference reactor *Plasma Sources Sci. Technol.* **8** 534–43
[27] Holstein T 1947 Imprisonment of resonance radiation in gases *Phys. Rev.* **72** 1212–33
[28] Molisch A F, Oehry B P, Schupita W and Magerl G 1993 Radiation-trapping in cylindrical and spherical geometries *J. Quant. Spectrosc. Radiat. Transfer* **49** 361–70
[29] Navrátil Z, Trunec D, Hrachová V and Kaňka A 2007 Collisional–radiative model of neon discharge: determination of E/N in the positive column of low pressure discharge *J. Phys. D: Appl. Phys.* **40** 1037
[30] Ivanov V A 1998 Electron-impact-induced excitation transfer between 3s levels of the neon atom *J. Phys. B: At. Mol. Opt. Phys.* **31** 1765
[31] Martin W C *et al* 2004 *NIST Atomic Spectra Database* http://physics.nist.gov/asd
[32] Seaton M J 1998 Oscillator strength in Ne I *J. Phys. B: At. Mol. Opt. Phys.* **31** 5315–36
[33] Vahedi V, DiPeso G, Birdsall C K, Lieberman M A and Rognlien T D 1993 Capacitive RF discharges modelled by particle-in-cell Monte Carlo simulation: I. Analysis of numerical techniques *Plasma Sources Sci. Technol.* **2** 261–72
[34] Verboncoeur J P, Alves M V, Vahedi V and Birdsall C K 1993 Simultaneous potential and circuit solution for 1D bounded plasma particle simulation codes *J. Comput. Phys.* **104** 321–8
[35] Vahedi V, Birdsall C K, Lieberman M A, DiPeso G and Rognlien T D 1993 Capacitive RF discharges modelled by particle-in-cell Monte Carlo simulation: II. Comparisons with laboratory measurements of electron energy distribution functions *Plasma Sources Sci. Technol.* **2** 273–8
[36] Longo S 2000 Monte Carlo models of electron and ion transport in non-equilibrium plasmas *Plasma Sources Sci. Technol.* **9** 468–76
[37] Hagelaar G and Kroesen G 2000 A Monte Carlo modelling study of the electrons in the microdischarges in plasma addressed liquid crystal displays *Plasma Sources Sci. Technol.* **9** 605–14
[38] Nagayama K, Farouk B and Lee Y 1998 Particle simulation of radio-frequency plasma discharges of methane for carbon film deposition *IEEE Trans. Plasma Sci.* **26** 125–34
[39] Lieberman M A and Lichtenberg A J 1994 *Principles of Plasma Discharges and Material Processing* (New York: Wiley)
[40] Lide D R 1999 *CRC Handbook of Chemistry and Physics* (Boca Raton, FL: CRC Press)
[41] Godyak V and Piejak R 1990 Abnormally low electron-energy and heating-mode transition in a low-pressure argon RF discharge at 13.56 MHz *Phys. Rev. Lett.* **65** 996–9
[42] Brzobohatý O and Trunec D 2006 Influence of the Ramsauer minimum on the plasma characteristics studied via computer simulation *Czech. J. Phys. (Suppl. B)* **56** B665–71
[43] Brzobohatý O, Buršíková V, Nečas D, Valtr M and Trunec D 2008 Influence of substrate material on plasma in

deposition/sputtering reactor: experiment and computer simulation *J. Phys. D: Appl. Phys.* **41** 035213

[44] Boffard J B, Keeler M L, Piech G A, Anderson L W and Lin C C 2001 Measurement of electron-impact excitation cross sections out of the neon $^3P_2$ metastable level *Phys. Rev.* A **64** 032708

[45] Behnke J F, Deutsch H and Scheibner H 1985 Investigation about stepwise excitation cross sections in rare gases *Contrib. Plasma Phys.* **25** 41

[46] Leveau J, Valignat S and Deigat F 1977 Destruction par chocs électroniques des atomes métastables et pseudo-métastables de néon dans une colonne positive *J. Phys.—Lett.* **38** L385